Activity-based RNA modifying enzyme probing reveals DUS3L-mediated dihydrouridylation

Wei Dai^{1,5}, Ang Li^{1,5}, Nathan J. Yu¹, Thao Nguyen^{2,3,4}, Robert W. Leach³, Martin Wühr^{2,3}, & Ralph E. Kleiner^{1*}

¹Department of Chemistry, Princeton University, Princeton, NJ 08544, USA

²Department of Molecular Biology, Princeton University, Princeton, NJ 08544, USA

³Lewis-Sigler Institute for Integrative Genomics, Princeton University, Princeton, NJ 08544, USA

⁴Department of Chemical and Biological Engineering, Princeton University, Princeton, NJ 08544, USA

⁵These authors contributed equally.

^{*}email: rkleiner@princeton.edu

ABSTRACT

Epitranscriptomic RNA modifications can regulate RNA activity, however there remains a major gap in our understanding of the RNA chemistry present in biological systems. Here, we develop RNA-mediated activity-based protein profiling (RNABPP), a chemoproteomic strategy relying upon metabolic RNA labeling, mRNA interactome capture, and quantitative proteomics, to investigate RNA-modifying enzymes in human cells. RNABPP with 5-fluoropyrimidines allowed us to profile 5-methylcytidine (m⁵C) and 5-methyluridine (m⁵U) methyltransferases. Further, we uncover a novel mechanism-based crosslink between 5-fluorouridine-modified RNA and the dihydrouridine synthase homolog DUS3L. We investigate the mechanism of crosslinking and use quantitative nucleoside LC-MS/MS analysis and 5-fluorouridine-based crosslinking and immunoprecipitation (CLIP) sequencing to map DUS3L-dependent dihydrouridine (DHU) modifications transcriptome-wide. Finally, we show that DUS3L KO cells have compromised protein translation rates and impaired cellular proliferation. Taken together, our work provides a general approach for profiling RNA modifying enzyme activity in living cells and reveals new pathways for epitranscriptomic RNA regulation.

Introduction

Post-synthetic modifications on biological macromolecules play important roles in biological processes. Among the central macromolecules of life, RNA exhibits perhaps the greatest diversity in modification chemistry¹. RNA modifications are conserved throughout biology and are critical for the proper function of tRNA and rRNA². In addition, studies from the last decade have revealed that mRNA is subject to diverse post-transcriptional modifications (known as the "epitranscriptome"). These modifications, best exemplified by N⁶-methyladenosine (m⁶A), can impact mRNA behavior and regulate gene expression³. Moreover, studies of epitranscriptomic modifications have indicated that their dysregulation may be involved in disease etiology⁴.

Our understanding of m^6A on RNA has been rapidly maturing, largely due to powerful technologies for mapping individual modification sites 5 and characterization of associated writer, eraser, and reader proteins 6 . In contrast, insights into other RNA modifications have accumulated more slowly. For example, modifications on pyrimidines, including 5-methylcytidine (m^5C), 5-methyluridine (m^5U), dihydrouridine (DHU), pseudouridine (ψ), and others, are abundant in non-coding RNA and conserved throughout evolution, but we lack insight into their biological role. For many modifications, progress has been hampered by a dearth of reliable strategies for mapping modifications transcriptome-wide and identifying writer enzymes, as is needed for functional studies. Further, while nature has evolved rich biosynthetic machinery for

modifying tRNA, the extent to which these modifications exist on mRNA is largely unknown.

Identifying RNA writer enzymes and their substrates is a major challenge, and these proteins are typically deduced based on homology or through screening. An alternative approach to enzyme discovery and profiling, known as activity-based protein profiling (ABPP)⁷, relies on reactive small-molecule probes that form covalent adducts with enzyme families based upon distinctive chemical features. ABPP provides a general platform for proteomic studies based upon chemical reactivity, but is typically limited to examples where a small molecule can mimic the native substrate, making challenging its application to RNA modifying enzymes.

Here, we develop RNA-mediated activity-based protein profiling (RNABPP) (**Figure 1a**), a reactivity-based approach to profile RNA modifying enzymes in living cells. RNABPP relies upon metabolic labeling with 5-fluorocytidine (5-FCyd) (**Figure 1b**), a cytidine analog that is efficiently incorporated into RNA and can form stable, mechanism-based adducts with RNA modifying enzymes. We combine this warhead with mRNA interactome capture^{8, 9} and quantitative mass spectrometry¹⁰ to profile RNA modifying enzymes in their native context. In addition to identifying mammalian m⁵C RNA methyltransferases, which are predicted to form crosslinks with 5-FCyd-containing RNA based upon their catalytic mechanism, our approach captures m⁵U methyltransferases as well as DUS3L, the mammalian homolog of yeast dihydrouridine synthase DUS3. We investigate the crosslinking mechanism to establish that 5-halopyrimidines can

function as activity-based probes for DUS3L. Further, we characterize its cellular RNA substrates using quantitative nucleoside LC-MS/MS and iCLIP-based sequencing¹¹. Finally, we show that DUS3L regulates cell proliferation and protein translation efficiency. Our work provides an unbiased, reactivity-based platform for RNA modifying enzyme discovery and characterization and expands our understanding of epitranscriptomic modifications in human RNA.

Main text

Metabolic labeling with 5-fluorocytidine (5-FCyd)

In order to develop our strategy (**Figure 1a**), we needed a versatile chemical warhead that is efficiently incorporated into cellular RNA and forms stable, covalent adducts with RNA modifying enzymes. For this purpose, we chose 5-FCyd, a mechanism-based inhibitor of RNA m⁵C methyltransferases¹² (**Figure 1b**). Since 5-FCyd is isosteric with cytidine, we reasoned that it should be efficiently incorporated into cellular RNA and minimally perturb recognition by RNA modifying enzymes. Further, we expected that adducts formed between 5-FCyd-RNA and m⁵C methyltransferases (**Figure 1b**) would be stable, in contrast to the widely used inhibitor 5-azacytidine (5-AzaC)¹³. Finally, we suspected that 5-FCyd would be deaminated in cells to generate 5-fluorouridine (5-FUrd)¹⁴, enabling reactivity-based profiling of enzymes modifying either cytidine or uridine.

To investigate metabolic labeling with 5-FCyd in cells, we employed quantitative LC-MS/MS. Gratifyingly, treatment of HEK293T cells with 5-FCyd for 12 h resulted in

efficient total RNA incorporation with 3% 5-FCyd/Cyd at 10 μM treatment and 13% 5-FCyd/Cyd at 100 μM treatment (**Figure 1c** and **Supplementary Table 1**) without overt cytotoxicity (**Supplementary Figure 1**). Further, we measured metabolic conversion of 5-FCyd to 5-FUrd, with 0.6% and 8% RNA labeling with 5-FUrd using 10 μM and 100 μM 5-FCyd treatment conditions, respectively (**Figure 1c** and **Supplementary Table 1**). Incorporation of 5-FCyd into mRNA proceeded with similar efficiency (**Supplementary Figure 2**).

Moving forward, we evaluated crosslinking between 5-FCyd-labeled RNA and m⁵C methyltransferases in cells. While 5-FCyd-modified RNA oligonucleotides crosslink with bacterial RNA m⁵C methyltransferases *in vitro*¹², cellular crosslinking has been typically accomplished using 5-AzaC¹³. To test 5-FCyd-mediated crosslinking, we expressed several m⁵C methyltransferases in HEK293T or Flp-In 293 cells including NSUN2, NSUN5, NSUN6, and DNMT2, treated cells with 5-FCyd, and evaluated RNA-protein crosslinking by western blot. In all cases, we observed a slower migrating band upon 5-FCyd-treatment (**Figure 1d**), consistent with crosslinking, and likely to abundant RNAs of uniform size, such as tRNA substrates of NSUN2, NSUN6 and DNMT2. Further, with NSUN2, we observed no crosslinking when 5-AzaC was used in place of 5-FCyd (**Figure 1e**), likely due to the instability of the 5-AzaC adduct.

Proteomic profiling of 5-FCyd-reactive proteins

After establishing 5-FCyd-m⁵C methyltransferase crosslinking in cells, we tested whether we could isolate crosslinked RNA-protein complexes for unbiased proteomic

analysis. For this purpose, we chose mRNA interactome capture^{8, 9}, which relies on oligo-dT hybridization to isolate protein-mRNA complexes (typically generated by photocrosslinking) directly from lysate. Since this approach should primarily enrich for mRNA m⁵C methyltransferases, we tested this strategy with NSUN2, which methylates both tRNA^{13, 15} and mRNA^{16, 17}. In brief, cells expressing epitope-tagged NSUN2 were treated with 5-FCyd for 12 hr and covalent RNA-protein complexes were isolated under denaturing conditions using oligo-dT-based pulldown. Following bead elution, we characterized polyA RNA enrichment using Bioanalyzer analysis (**Supplementary Figure 3**), and measured protein enrichment by western blot after RNA digestion. Gratifyingly, we were able to observe strong enrichment of NSUN2 in the 5-FCydtreated cells compared to control cells or those treated with 5-AzaC (**Figure 1e**), establishing that metabolic labeling with 5-FCyd combined with oligo-dT-based enrichment can be applied to isolate mRNA modifying enzymes.

Having validated our approach, we next profiled 5-FCyd-reactive proteins using quantitative mass spectrometry-based proteomics. We set up a comparative analysis pipeline to measure protein enrichment in 5-FCyd-treated cells compared to untreated cells. Independent samples were labeled with TMT-based isobaric tags¹⁸ and quantified in one LC-MS/MS run (**Figure 2a and Supplementary Dataset 1**). In total, we found nine proteins enriched with p value < 0.05 – all but one are known or putative pyrimidine modifying enzymes. Of these, four are m⁵C methyltransferases including NSUN2^{16, 17}, which we used to validate the method. We also identified NSUN5, NSUN5C, and DNMT2. NSUN5/NSUN5C are the mammalian homologues of Rcm1, a yeast rRNA

m⁵C methyltransferase¹⁹. Recently, it was found that NSUN5 methylates analogous residues in human rRNA²⁰; its activity on other RNA species is unexplored although it can bind to G-quadruplex structures in NRAS mRNA²¹. DNMT2 homologs have been primarily implicated in m⁵C formation at C38 on tRNA²², although recent evidence has implicated human DNMT2 in mRNA modification²³.

The 5-FCyd-treated samples also showed enrichment of several enzymes likely to modify uridine. Since 5-FCyd feeding generates 5-FUrd in RNA, these proteins are likely captured by 5-FUrd. TRMT2A and TRMT2B are the mammalian homologues of yeast TRM2²⁴, and were recently shown to install 5-methyluridine (m⁵U) at U54 on cytosolic²⁵ and mitochondrial tRNAs²⁶, respectively. These proteins use a similar catalytic mechanism as m⁵C methyltransferases²⁵, and should crosslink with 5-FUrd-modified RNA. Our data suggests that these proteins may generate m⁵U on mRNA, consistent with a recent finding by Feng and co-workers²⁷. Finally, we were surprised to find DYPD and DUS3L, enzymes from the dihydropyrimidine dehydrogenase family and tRNA-dihydrouridine synthase family, respectively, enriched upon 5-FCyd treatment.

Both of these enzymes should catalyze a similar reaction – reduction of C5-C6 double bond of uracil – but DYPD²⁸ is known to modify the free nucleobase and DUS3L is predicted to modify tRNA by homology to yeast DUS3²⁹. Notably, dihydrouridine (DHU) has not previously been reported to occur on human mRNA.

Characterization of m⁵C and m⁵U methyltransferases

To further explore our findings, we validated interactions of our top hits, NSUN2, NSUN5, and TRMT2A, with mRNA by analyzing crosslinking and protein recovery by western blot. Gratifyingly, we were able to recover all three proteins using the RNABPP workflow, validating our proteomics results (**Figure 2b, Supplementary Figure 4** and **Supplementary Figure 5**). For TRMT2A, we also observed protein-RNA crosslinking upon 5-FUrd feeding (**Figure 2c**) and TRMT2A could be recovered using 5-FUrd RNABPP (**Supplementary Figure 6a**) – suggesting that this enzyme was most likely enriched by metabolic conversion of 5-FCyd to 5-FUrd.

Next, we characterized the contributions of NSUN2, NSUN5, and TRMT2A to cellular m⁵C and m⁵U formation. We generated KO cells for each gene using CRISPR/Cas9 technology (**Supplementary Table 2**, **Supplementary Figures 7** and **8**), extracted RNA, and measured m⁵C and m⁵U modification levels by nucleoside LC-MS/MS. A rigorous purification protocol employing double polyA pulldown and small RNA and rRNA depletion was used to prepare the mRNA fraction (**Figure 3a and Supplementary Figure 9a**). We monitored N⁶-isopentenyladenosine levels (i⁶A), which is characteristic to tRNA³⁰, to ensure efficient depletion of small RNA (**Supplementary Figures 9 b and c**). Consistent with previous RNA bisulfite sequencing and m⁵C mass spectrometry that have implicated NSUN2 as the major mRNA m⁵C-forming enzyme¹⁶.

17, we found an 82% reduction in mRNA m⁵C levels upon NSUN2 knockout (**Figure 3c**, **Supplementary Figures 10 and 11, Supplementary Tables 3** and **4**)¹⁷. We also found that NSUN2 installs the majority of m⁵C sites on total RNA (76% reduction upon NSUN2 KO) (**Figure 3b**), likely reflective of abundant tRNA m⁵C sites^{13, 15}. While our LC-MS/MS

data together with published sequencing maps^{16, 17} support the existence of NSUN2-dependent m⁵C sites on mRNA, interpretation of nucleoside LC-MS data from polyA-enriched fractions must be treated carefully. We have employed a rigorous polyA mRNA purification, however since m⁵C is ~40-fold higher in total RNA than polyA-RNA, and comparably reduced in each sample upon NSUN2 KO (**Figure 3b and 3c**), we cannot exclude the possibility that contaminating tRNA/rRNA nucleosides may contribute to the measured m⁵C content.

We next investigated the contribution of NSUN5 and TRMT2A to m⁵C formation. We found no statistically significant change in m⁵C levels upon knockout of either protein (**Figure 3b, 3c**). This is not unexpected for TRMT2A, which is a known m⁵U methyltransferase and likely enriched by 5-FUrd. NSUN5 has been shown to generate m⁵C at a single rRNA site through bisulfite mapping approaches²⁰, and our data suggest it is unlikely to have many additional substrates. It is also plausible that 5-FCyd-NSUN5 crosslinks occur through kinetic trapping of the enzyme-RNA complex, and do not reflect bonafide m⁵C modification.

The identification of m⁵U methyltransferases TRMT2A and TRMT2B in our dataset suggests the presence of m⁵U on human mRNA. To investigate further, we performed LC-MS/MS analysis of m⁵U levels in RNA extracted from WT HEK293T and TRMT2A KO cells as described above (**Supplementary Tables 3** and **4**). In total RNA, we found a dramatic decrease in m⁵U upon TRMT2A knockout, with 95% reduction of the modification (**Figure 3d**), consistent with published data²⁵. Further, we detected m⁵U in

the enriched mRNA fraction, albeit at lower levels than in total RNA, and observed a 59% reduction of m⁵U upon TRMT2A knockout (**Figure 3e**). Our results suggest that TRMT2A may install m⁵U on cellular mRNA, consistent with a recent study²⁷. In addition, residual m⁵U in the mRNA-enriched fraction upon TRMT2A ablation suggests the existence of other m⁵U methyltransferases. We propose that TRMT2B is a likely candidate, given its enrichment in our proteomic dataset and evidence that it modifies tRNA and rRNA²⁶. At the current time, however, given the lack of sequencing data supporting the existence of m⁵U on mRNA and the low levels of this modification measured in polyA-enriched RNA fractions as compared to high levels in non-coding RNAs, nucleoside LC-MS data alone should be treated cautiously³¹.

5-halopyrimidines crosslink DUS3L

We next turned to DUS3L, the mammalian homolog of yeast dihydrouridine synthase DUS3²⁹. Phizicky and co-workers previously demonstrated that yeast DUS3 installs dihydrouridine (DHU) at U47 in tRNA^{Tyr29}, however, its mammalian homolog, DUS3L, has been uncharacterized and we lack transcriptome-wide maps of DHU sites in any organism. Further, to our knowledge, DHU has been found exclusively in tRNA and rRNA, and there is no precedent for its occurrence in mRNA. To probe our finding further, we analyzed crosslinking and RNABPP protein enrichment with an anti-DUS3L antibody. In lysate generated from 5-FCyd treated cells, we observed slower migrating species (**Figure 4a**), consistent with covalent RNA-protein adducts. Further, in 5-FCyd labeled samples but not in the control, we were able to detect DUS3L after oligo-dT pulldown (**Figure 4a**, **Supplementary Figure 12**). Taken together, these results

demonstrate 5-FCyd-dependent RNA crosslinking of DUS3L and support its interaction with polyadenylated RNA.

Next, we investigated the RNA-protein crosslinking mechanism. Since DUS enzymes modify uridine, we tested whether metabolic labeling with 5-FUrd would result in crosslinking and protein enrichment. Our results demonstrate similar amounts of crosslinking (Figure 4b) and protein recovery (Supplementary Figure 6b) using either 5-FCyd or 5-FUrd, which are suggestive of 5-FUrd as the major crosslinking entity. We also evaluated crosslinking with modified pyrimidine analogs containing chloro or bromo groups at the C5 position. In all cases, we observed efficient DUS3L crosslinking (Figure 4b). How do 5-halopyrimidines facilitate crosslinking of DUS3L? Based on structural and biochemical data for DUS enzymes^{32, 33}, we propose that crosslinking begins with enzymatic reduction of 5-halouridine to 5-halodihydrouridine followed by nucleophilic attack of a conserved catalytic Cys (C396 in DUS3L) on the C5 position with halide serving as leaving group (Figure 4c). To directly test this hypothesis, we generated a stable DUS3L KO cell line (Supplementary Figures 7 and 8) using CRISPR/Cas technology and transfected plasmids encoding either WT DUS3L or DUS3L containing the C396A mutation. Following feeding with 5-FUrd or 5-BrUrd, we were able to observe crosslinking to the WT transgene, but not to the C396A mutant, suggesting that the catalytic Cys residue is important for crosslinking. (Figure 4d)

LC-MS quantification of DHU levels in human RNA

We next studied the role of DUS3L in cellular DHU formation. We isolated RNA from WT and two independent DUS3L KO cell lines generated using CRISPR/Cas technology and measured DHU levels in total RNA, mRNA, and small RNA using LC-MS/MS (Supplementary Figures 13, 14, 15; Supplementary Tables 5, 6, 7). In total RNA, we found an appreciable level of DHU, corresponding to 0.8% of all uridine residues. Interestingly, DHU levels in total RNA of both DUS3L KO strains were largely unchanged relative to WT, indicating that DUS3L catalyzes a minor fraction of DHU modification on total RNA (Figure 4e) – it is likely that the majority of DHU is installed by the other mammalian DUS homologs (i.e. DUS1L, DUS2L, and DUS4L). In the small RNA fraction (17 to 300 nt), which contains tRNA, we observed a dramatically higher level of DHU, corresponding to ~8% of total uridine residues (Figure 4f), and an 18% decrease in DHU levels in the DUS3L KO strains (Figure 4f), establishing a role for DUS3L in DHU formation, most likely on mammalian tRNA. This would be analogous to yeast DUS3, which modifies U47 on yeast tRNA^{Tyr 29}. Further, we isolated mRNA from WT and DUS3L KO strains using the previously described approach and analyzed DHU levels. We detected DHU in the mRNA-enriched fraction, although levels were far lower than in total RNA and small RNA. Interestingly, despite modest decrease of DHU in total RNA or small RNA upon DUS3L KO, we observed a 60-70% decrease in DHU levels in polyA-enriched RNA for both DUS3L KO strains. While this data does support the existence of DHU on human mRNA (Figure 4g), given the extremely low levels that we measure, and the possibility of contaminating DHU from abundant non-coding RNA species, further evidence is needed to unambiguously establish the presence of DHU on human mRNA.

Mapping DUS3L-dependent DHU sites

Since the biological substrates of DUS3L are unknown, we adapted the iCLIP method¹¹ to map DUS3L-dependent DHU sites transcriptome-wide using metabolic labeling with 5-FUrd to crosslink substrate RNAs (Figure 5a). Analogous approaches have been applied to map m⁵C and m⁵U methyltransferase substrates using metabolic labeling with modified pyrimidines^{13, 25} or methyltransferase variants that cannot release RNA substrate¹⁵. In brief, we fed cells with 5-FUrd and immunoprecipitated DUS3L together with covalently linked RNA. Analysis of DUS3L-associated RNA demonstrated clear enrichment over cells not treated with 5-FUrd or cells expressing C396A DUS3L (Figure 5b and Supplementary Figure 16a), indicating the specificity of RNA-protein crosslinking. Next, we generated iCLIP libraries from 5-FUrd treated cells following literature precedent (Supplementary Figures 16b and 16c)³⁴. Control RNA libraries were prepared from untreated cells expressing WT DUS3L. Based upon the number of PCR cycles required to generate detectable PCR product, we estimate ~10-fold more RNA in the 5-FUrd-treated samples as compared to control. RNA libraries were subjected to Illumina sequencing and deduplicated and uniquely aligned reads were used to identify crosslink sites based upon reverse transcription stop signatures. Crosslink sites were further aggregated into crosslink peaks using Paraclu³⁵, and only peaks present in multiple independent biological replicates and showing at least 4-fold enrichment over the control were used for further analysis (Supplementary Dataset 2).

Analysis of 5-FUrd-treated DUS3L samples showed that the largest fraction of unique reads mapped to cytoplasmic tRNA genes (Figure 5c). In contrast, the majority of reads in control samples originated from rRNA, likely reflecting non-specific binding (Supplementary Figure 16d). In total, we identified 180 tRNA peaks corresponding to 45 different tRNA isoacceptors (Figure 5d, Supplementary Dataset 2). Further, alignment of all tRNA peaks according to their relative position within the mature tRNA transcript demonstrated strong enrichment at positions 45-47(Figure 5e and **Supplementary Dataset 2**) with 28 of the 45 tRNA isoacceptors containing peaks between positions 44-49 (Supplementary Dataset 2). Since the nearest U residue occurs at position 46-48 in most tRNAs, we conclude that DUS3L reacts with 5-FUrd at residues U46-48 and reverse transcription proceeds on average 1 additional nucleotide into the DUS3L-RNA crosslinked adduct. In addition, we observed minor peaks near position 58, likely due to abundant m¹A modification at this position, as well as 5' to the U46-48 site, which may result from partial read-through of the DUS3L-5-FUrd adduct (Figure 5e, Supplementary Dataset 2). MEME³⁶ analysis of the crosslink peaks identified a consensus motif that matches the variable loop sequence of many tRNA isoacceptors (Figure 5f). Taken together, our iCLIP data show that U46-48 in the tRNA variable loop is a major dihydrouridylation site for human DUS3L. Phizicky and coworkers²⁹ reached a similar conclusion in their studies of yeast DUS3 with individual tRNAs, indicating that the tRNA modifying function of this enzyme is conserved in eukaryotic evolution.

Since we identified DUS3L through RNABPP oligo-dT pulldown and measured DHU in the polyA RNA fraction, we also investigated DUS3L peaks mapping to non-tRNA genes. Among different classes of RNA identified in the 5-FUrd treated samples, we found ~2-fold increase in the fraction of uniquely mapped reads from mRNA and IncRNA as compared to the control (Figure 5c, Supplementary Figure 16d) and identified 830 total non-tRNA crosslink peaks (Supplementary Dataset 2). Most of these peaks mapped to introns and non-coding RNA, and on average showed ~10-fold lower normalized read count than DUS3L tRNA peaks (Supplementary Dataset 2). Among non-tRNA peaks, we found 80 peaks in mature mRNA transcripts, distributed evenly across 5' and 3'-UTRs and coding sequences (Supplementary Dataset 2, **Supplementary Figure 16e**). Another 44 peaks were located in retained introns, which can be incorporated into mature transcripts. MEME analysis of mRNA peaks yielded the consensus motif GGGTCC (Supplementary Figure 16f), similar to the tRNA DHU site at residues 46-48. While these peaks do suggest DHU modification in mRNA, given the propensity of RT-stop based analyses for generating false positives³¹ and the relatively low number and abundance of these peaks, orthogonal validation will be required to firmly establish DUS3L-mediated DHU modifications outside of the tRNA variable loop.

DUS3L regulates protein translation and cell viability

Having mapped the cellular substrates of DUS3L, we next studied the effect of DUS3L knockout on protein translation and cell viability. In order to measure protein translation rate, we fed WT and DUS3L KO cells O-propargyl-puromycin (OP-puro)³⁷ and measured its accumulation into cellular proteins using fluorescence microscopy and

flow cytometry. In DUS3L KO strains, we observed 18 – 23% reduction in OP-puro labeling (**Figures 6a, 6b** and **6c; Supplementary Table 8**), indicating that protein translation was impaired in these cell lines, and implicating DUS3L in this process. We also found that DUS3L exhibited primarily nuclear localization (**Figure 6a**). To quantify cell growth and metabolism, we utilized an MTS-based assay and observed a 40% reduction in viability in both DUS3L KO strains after 3 days (**Figure 6d** and **Supplementary Table 9**). Given that we have identified widespread DUS3L-mediated dihydrouridylation in the tRNA variable loop, it is likely that the observed effects on protein translation and cell proliferation in DUS3L KO cells are a result of global hypomodification of tRNAs. Kato *et al.* ³⁸ previously demonstrated that hDUS2 knockdown impaired the growth of lung cancer cells, reinforcing the importance of dihydrouridine modification and DUS enzymes in fundamental cellular processes.

Discussion

In this manuscript, we develop an activity-based profiling strategy to study RNA modifying enzymes in living cells. While activity-based protein profiling has been applied to diverse classes of cellular enzymes⁷, its application to RNA modifying enzymes, an emerging class of disease-relevant pharmacologic targets, has been limited. Here, by applying metabolic labeling with 5-FCyd, we profile 3 distinct classes of pyrimidine modifying enzymes – m⁵C RNA methyltransferases, m⁵U RNA methyltransferases, and dihydrouridine synthases. The versatility of 5-FCyd is made possible by its partial conversion to 5-FUrd in cells, as well as diverse reactivity modes including latent electrophilicity and inhibition of β-elimination during enzyme-substrate release.

The presence of mRNA m⁵C and the identity of its writers has been controversial. While tRNA m⁵C sites have been well established^{13, 15, 22, 39}, RNA bisulfite sequencing of mRNA has led to inconsistent m⁵C maps⁴⁰ and CLIP-based studies with NSUN2 have primarily identified tRNA modification sites^{13, 15}. Here, we provide two complementary data points supporting the existence of m⁵C on mRNA and implicating NSUN2 as its writer. First, we recover NSUN2 using oligo-dT-based pulldown with 5-FCyd. Second, LC-MS/MS analysis of polyA-enriched RNA demonstrates the NSUN2-dependent presence of m⁵C at levels of ~1 in 5,000 cytidine bases. LC-MS analysis of bulk nucleoside digests has known limitations in quantifying modification levels³¹, particularly when modifications are more abundant in tRNA/rRNA than in mRNA (as is the case for m⁵C). In addition, oligo-dT-based pulldown approaches can recover non-mRNA associated proteins. Therefore, while neither of these measurements alone is conclusive, they are consistent with 2 recent bisulfite sequencing studies that show NSUN2 is the major mRNA m⁵C writer^{16, 17}.

RNABPP with both 5-FCyd and 5-FUrd identified the m⁵U methyltransferase TRMT2A. In addition, we were able to detect m⁵U in bulk nucleoside digests from polyA-enriched RNA, although levels were ~10-fold lower than m⁵C. Recent work using CLIP-based sequencing has shown that TRMT2A primarily installs m⁵U U54 on tRNA, but did not identify TRMT2A-dependent m⁵U sites on mRNA²⁵, although a small number of mRNAs were found to associate with the protein. Similar to our study, Feng and co-workers measured m⁵U in bulk nucleoside digests from polyA-enriched RNA by mass

spectrometry. However, they did not observe a substantial reduction in m⁵U levels upon siRNA-mediated knockdown of TRMT2A²⁷ (perhaps due to inefficient knockdown). Given these contradictory findings, and the lack of sequencing strategies for profiling m⁵U sites transcriptome-wide, at the present time we feel that the existence of m⁵U on mRNA awaits further confirmation.

DHU is an abundant RNA modification found in all kingdoms of life⁴¹⁻⁴⁴. Yet, our understanding of this modified base in mammals is lacking. Our work provides the first transcriptome-wide characterization of the substrates of a mammalian dihydrouridine synthase. Taken together, LC-MS analysis of fractionated RNA in WT and DUS3L KO cells and sequencing of 5-FUrd-induced DUS3L-RNA crosslinks indicate that U46-48 in the tRNA variable loop is the major dihydrouridylation substrate of DUS3L. Our results align with studies by Phizicky and co-workers on yeast DUS3²⁹, which used microarray analysis to implicate the enzyme in DHU formation at U47 on a small number of tRNAs including tRNA^{Tyr}, tRNA^{Val}, tRNA^{Cys}, tRNA^{Ile}, tRNA^{Trp}, tRNA^{Thr}, and tRNA^{Asn}; modification of tRNA^{Tyr} was further confirmed by primer extension analysis. Our analysis of human DUS3L identified U46-48 sites on 28 tRNA isoacceptors including all of the tRNAs identified by the Phizicky study with the exception of tRNA^{Trp}. We did not identify any major DUS3L peaks in the DHU-rich "D-arm", which indicates that other mammalian DUS enzymes likely install DHU at these sites. Interestingly, while we observed reduced cell proliferation and protein translation in human DUS3L KO cells, DUS3 deletion alone in budding yeast does not cause overt growth defects²⁹, except when it is combined with the deletion of other tRNA modifying enzymes⁴⁵. This may be due to an increased

reliance upon dihydrouridylation in mammals for regulating tRNA structure, context-specific roles in the evaluated cell lines, as well as potential differences in the ability of yeast and mammalian enzyme to modify non-tRNA substrates. Notably, our 5-FUrd-iCLIP data shows DUS3L crosslinking peaks on non-tRNA substrates including a small number found in mature mRNA. While these peaks suggest potential DUS3L-catalyzed DHU modification sites on mammalian mRNA, given the relatively low abundance of reads at DUS3L mRNA peaks as compared to DUS3L tRNA peaks, and the indirect nature of reverse-transcription-stop based analyses³¹, orthogonal validation will be required to establish the existence of DHU on mammalian mRNA. Further investigation of DHU sites transcriptome-wide at single-nucleotide resolution will likely require the development of DHU-specific sequencing technology, analogous to approaches that have been deployed for other epitrancriptomic bases⁵ and will be critical to further understand the role that this modification and associated proteins play in biological processes.

Our study demonstrates an unexpected reactivity of DUS enzymes towards electrophilic nucleotides. Since most DUS enzymes possess a catalytic Cys residue, metabolically incorporated 5-halopyrimidines may serve as a general class of activity-based probes for the entire family, providing a chemical strategy for profiling DUS activity and substrate scope *in vivo*. In addition, Cys reactivity found in DUS enzymes⁴⁶ may be a starting point for the development of small molecule tools for this enzyme class^{47, 48}. We also envision that the modified nucleosides used in this work can be incorporated into synthetic oligonucleotides to develop probes for studying and modulating RNA

modifying enzyme activity *in vitro* and *in vivo*. Finally, with appropriate nucleoside selection, we propose that RNABPP can be applied broadly in a targeted (mechanismbased) or non-targeted (reactivity-based) manner to profile diverse RNA-associated protein in different biological contexts as well as at amino acid resolution⁴⁹. Electrophilic small-molecule ABPP probes have seen widespread use⁴⁷ and placement of these functional groups at the C5 position of pyrimidines should enable their integration into the RNABPP method. Such studies are underway in our group and will provide new insights into transcriptomic and epitranscriptomic processes in biology.

Acknowledgements

We thank Christina DeCoste and Katherine Rittenbach at the Princeton University Flow Cytometry Resource Facility for assistance with flow cytometry analysis. We thank Lillia Ryazanova (supported by the Princeton Catalysis Initiative and the Lewis-Sigler Collaboration Fund) for technical assistance. R.E.K. acknowledges support from a National Science Foundation CAREER award (MCB-1942565), the National Institute of Health (R01GM132189), the Sidney Kimmel Foundation, and the Alfred P. Sloan Foundation. This work was supported by NIH grant R35 GM128813 (to M.W.). T. N. was supported by the American Heart Association. W. D. was generously supported by the Edward C. Taylor 3rd Year Graduate Fellowship in Chemistry. A. L. was supported by the Princeton Catalysis Initiative. All authors thank Princeton University for financial support.

Author Contributions

R. E. K. conceived the study, analyzed data, wrote the manuscript, and performed experiments. W. D. performed RNABPP experiments, nucleoside mass spectrometry, crosslinking studies, and protein translation assays. A. L. performed iCLIP experiments and bioinformatic analysis. R. W. L. performed bioinformatic analysis. N. J. Y. performed cell viability assays and crosslinking studies. T. N. performed mass spectrometry proteomics and associated data analysis. M. W. supervised T. N.

Competing Financial Interests Statement

The authors declare no competing financial interest.

Figure Legends

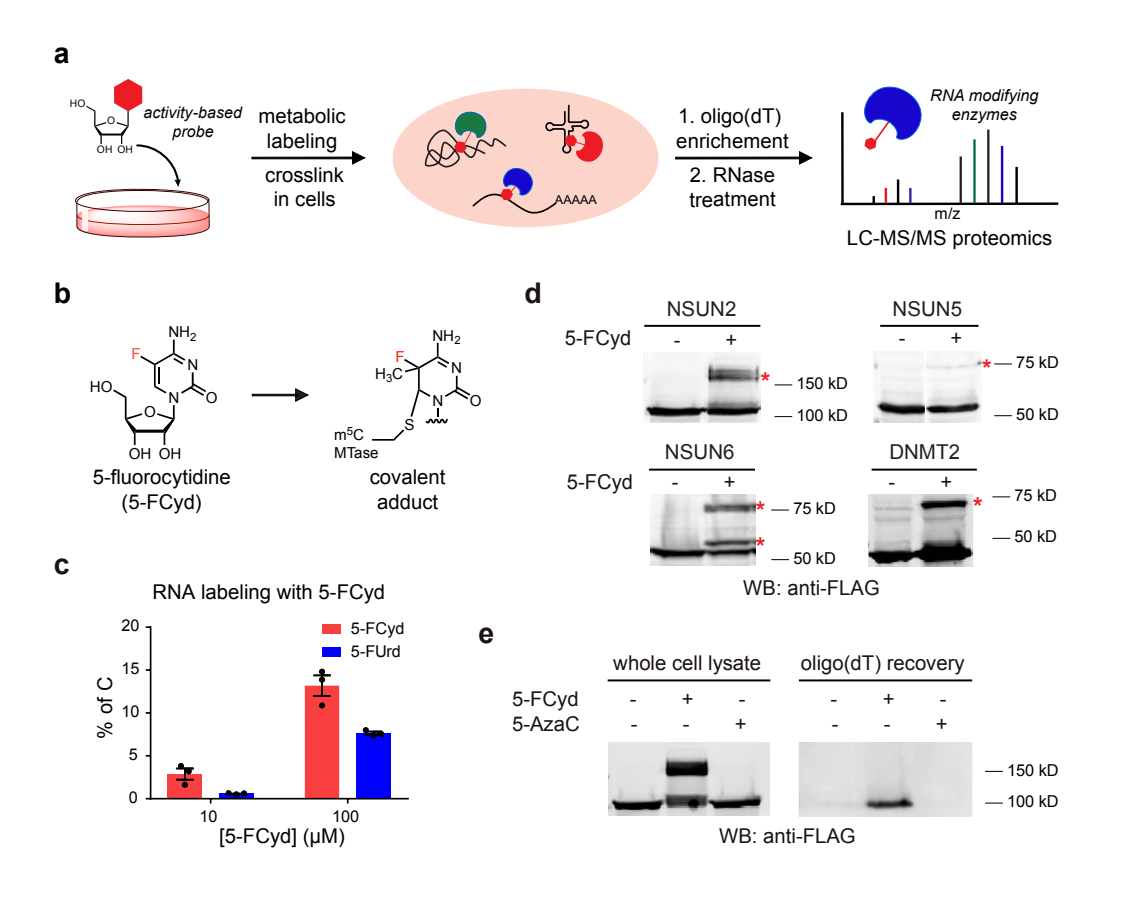


Figure 1. RNA-mediated activity-based protein profiling (RNABPP) enables the chemoproteomic analysis of RNA modifying enzymes in living cells. (a) Schematic representation of the RNABPP approach. Metabolic labeling with a nucleoside-based activity probe facilitates the incorporation of a chemical "warhead" into cellular RNA. Crosslinked RNA modifying enzymes on mRNA can then be identified through oligo-dT based enrichment and quantitative proteomics analysis. (b) Chemical structure of 5-FCyd and proposed RNA-protein crosslinking between 5-FCyd-labeled RNA and m⁵C RNA methyltransferases. (c) LC-MS/MS analysis of 5-FCyd and 5-FUrd levels in total RNA after metabolic labeling of HEK293T cells for 12 hr with 5-FCyd. 3 independent biological replicates were analyzed. Data represent mean values ± SEM. (d) Western blot analysis of protein-RNA crosslinking in cells after 5-FCyd labeling. NSUN2, NSUN5, NSUN6, and DNMT2 were expressed as 3xFLAG-fusion proteins and cells were treated with 10 µM 5-FCyd (for NSUN2 and NSUN6) and 100 µM 5-FCyd (for DNMT2 and NSUN5) for 12 hr. (e) Oligo-dT based isolation of NSUN2 using RNABPP with 5-FCyd. Cells were fed with 10 μM 5-FCyd, 10 μM 5-azacytidine (5-AzaC), or untreated, and subjected to the RNABPP workflow. For (d) and (e), the experiments were repeated 3 times independently with similar results.

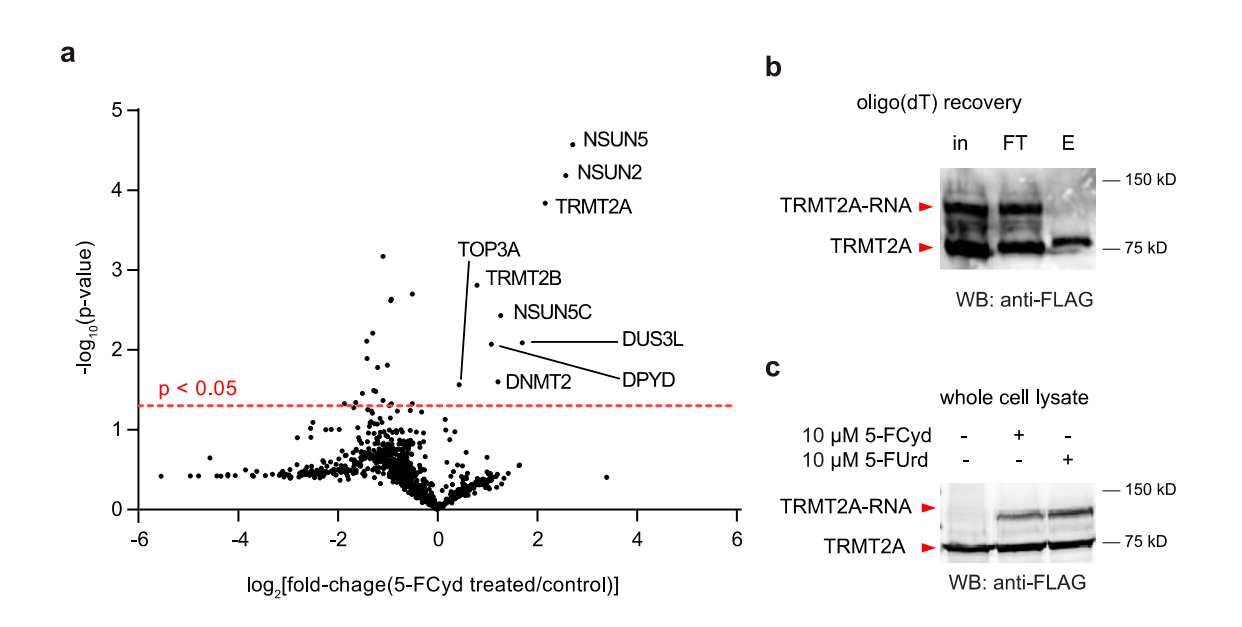


Figure 2. Proteomic analysis of 5-FCyd-reactive proteins on mRNA using RNABPP. **(a)** Volcano plot showing enrichment of 5-FCyd-reactive proteins. 3 independent biological replicates were analyzed using TMT-based isobaric tags. Multiple t test (unpaired) was performed to evaluate the statistical significance. P = 0.000065 for NSUN2; p = 0.000027 for NSUN5; p = 0.00015 for TRMT2A; p = 0.0015 for TRMT2B; p = 0.0037 for NSUN5C; p = 0.0081 for DUS3L; p = 0.0084 for DPYD; p = 0.025 for DNMT2; p = 0.027 for TOP3A. **(b)** Western blot validation of proteomics result for m⁵U methyltransferase TRMT2A. **(c)** Western blot analysis of TRMT2A-RNA crosslinking after metabolic labeling with 10 μM 5-FCyd or 5-FUrd for 12h. For (b) and (c), the experiments were repeated 3 times independently with similar results.

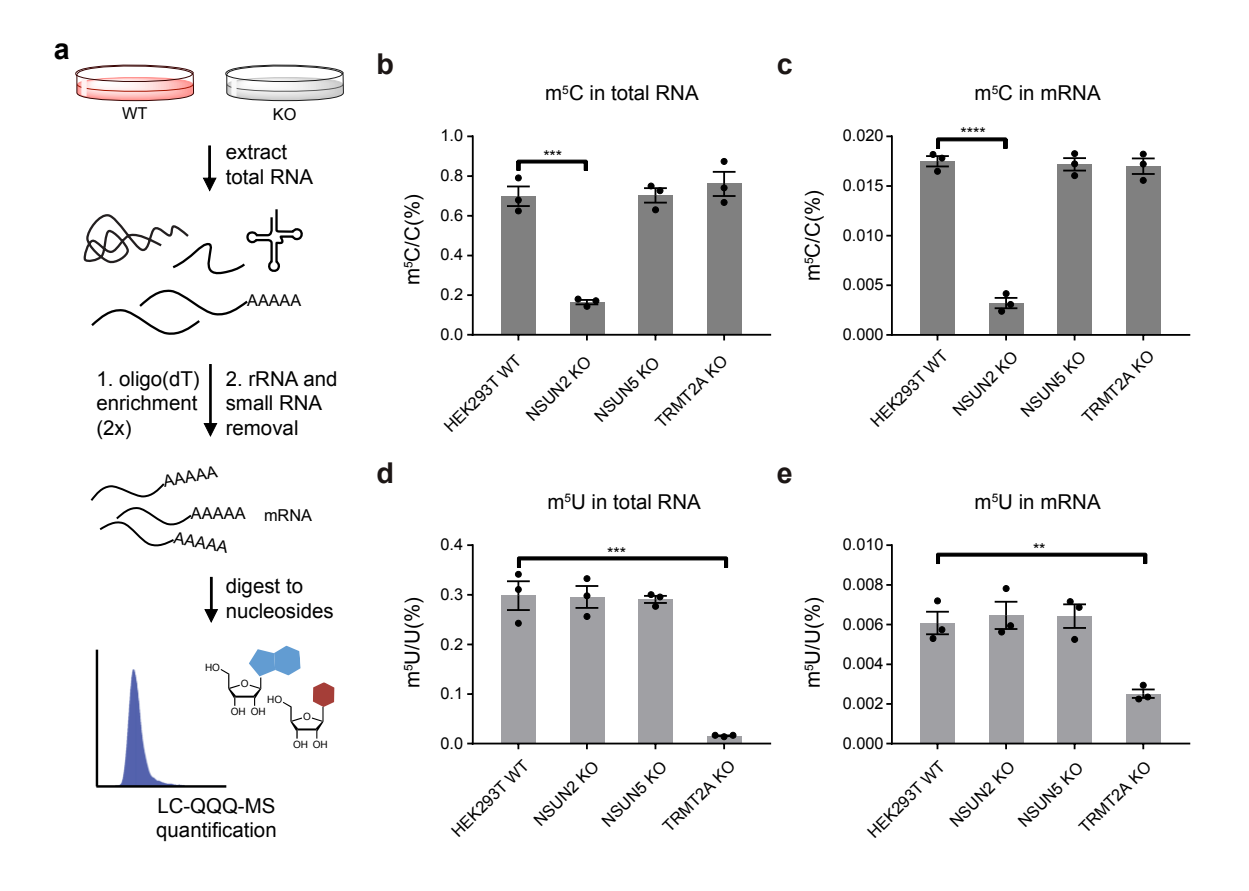


Figure 3. NSUN2 and TRMT2A are the major RNA m⁵C and m⁵U methyltransferases, respectively. **(a)** Schematic representation of mRNA isolation protocol for LC-QQQ-MS quantitation of modified nucleotides in HEK293T WT and KO cells. **(b)** - **(e)** Quantitation of m⁵C and m⁵U levels in total RNA and mRNA extracted from WT, NSUN2 KO, NSUN5 KO, and TRMT2A KO cell lines. 3 independent biological replicates were analyzed. Data represent mean values \pm SEM. Unpaired t test (two-tailed) was performed to evaluate the statistical significance. P = 0.00045 in (b); p = 0.000040 in (c); p = 0.00063 in (d).

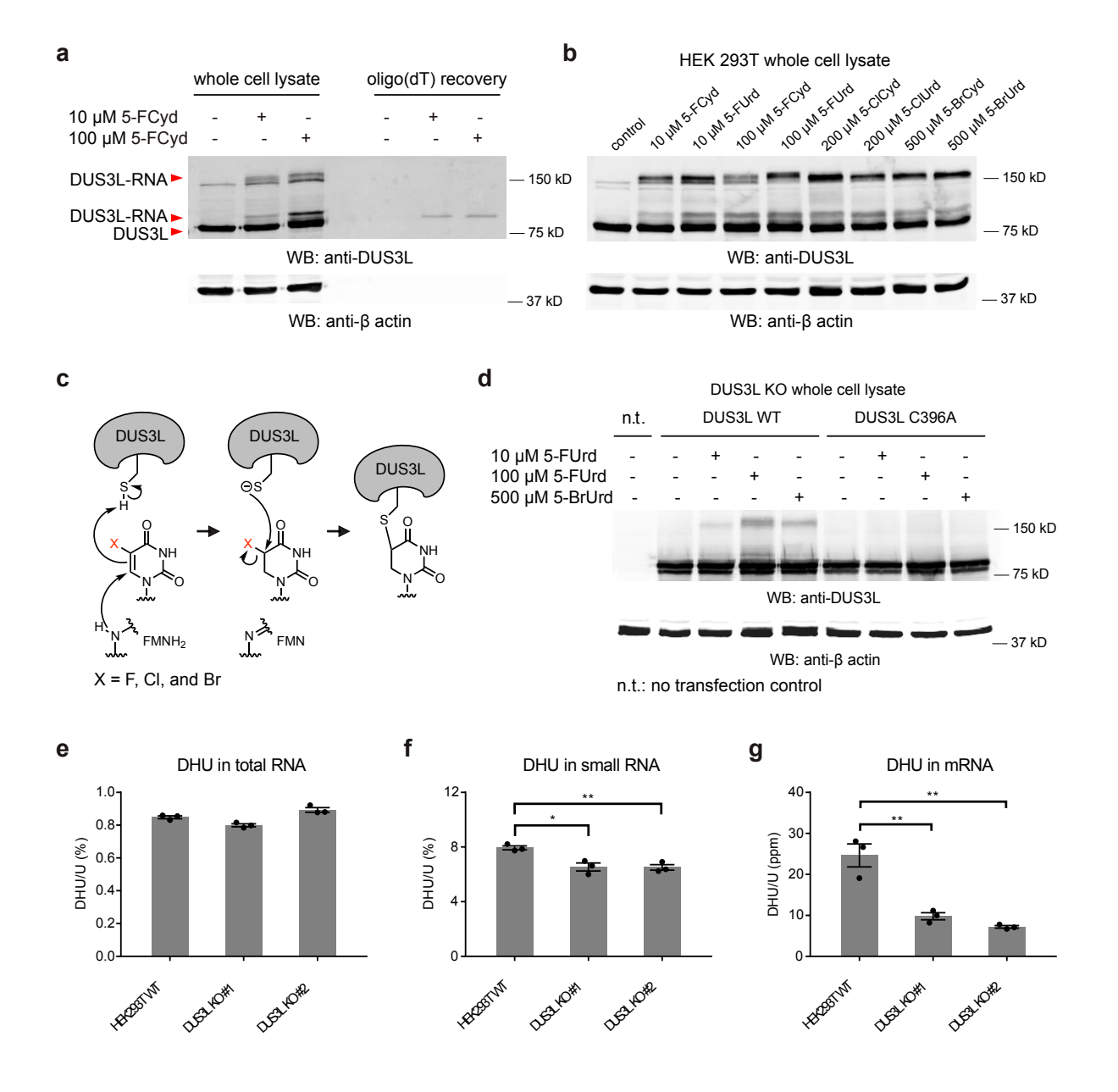


Figure 4. DUS3L installs dihydrouridine on human RNA. **(a)** Western blot analysis of 5-FCyd-mediated enrichment for DUS3L. After metabolic labeling with 5-FCyd, oligo-dT enriched samples were analyzed by western blot using an anti-DUS3L antibody. **(b)** Western blot analysis of DUS3L-RNA crosslinking after metabolic labeling with a panel of C5-halogenated pyrimidines. **(c)** Proposed mechanism of DUS3L-RNA crosslinking mediated by C5-halogenated uridine derivatives. **(d)** Western blot analysis of protein-RNA crosslinking between WT DUS3L or C396A DUS3L and 5-FUrd or 5-BrUrd labeled RNA. WT or mutant DUS3L transgenes were introduced by transfection of plasmid constructs into DUS3L KO cells. For (a), (b) and (d), the experiments were repeated 3 times independently with similar results. **(e) – (g)** Quantitation of dihydrouridine (DHU) levels in total RNA, small RNA, and mRNA extracted from WT and DUS3L KO cells. 3 independent biological replicates were analyzed. Data represent mean values \pm SEM. Unpaired t test (two-tailed) was performed to evaluate the statistical significance. *: p = 0.012, **: p = 0.0046 in (f); **: p = 0.0072 (#1) and p = 0.0035 (#2) in (g).

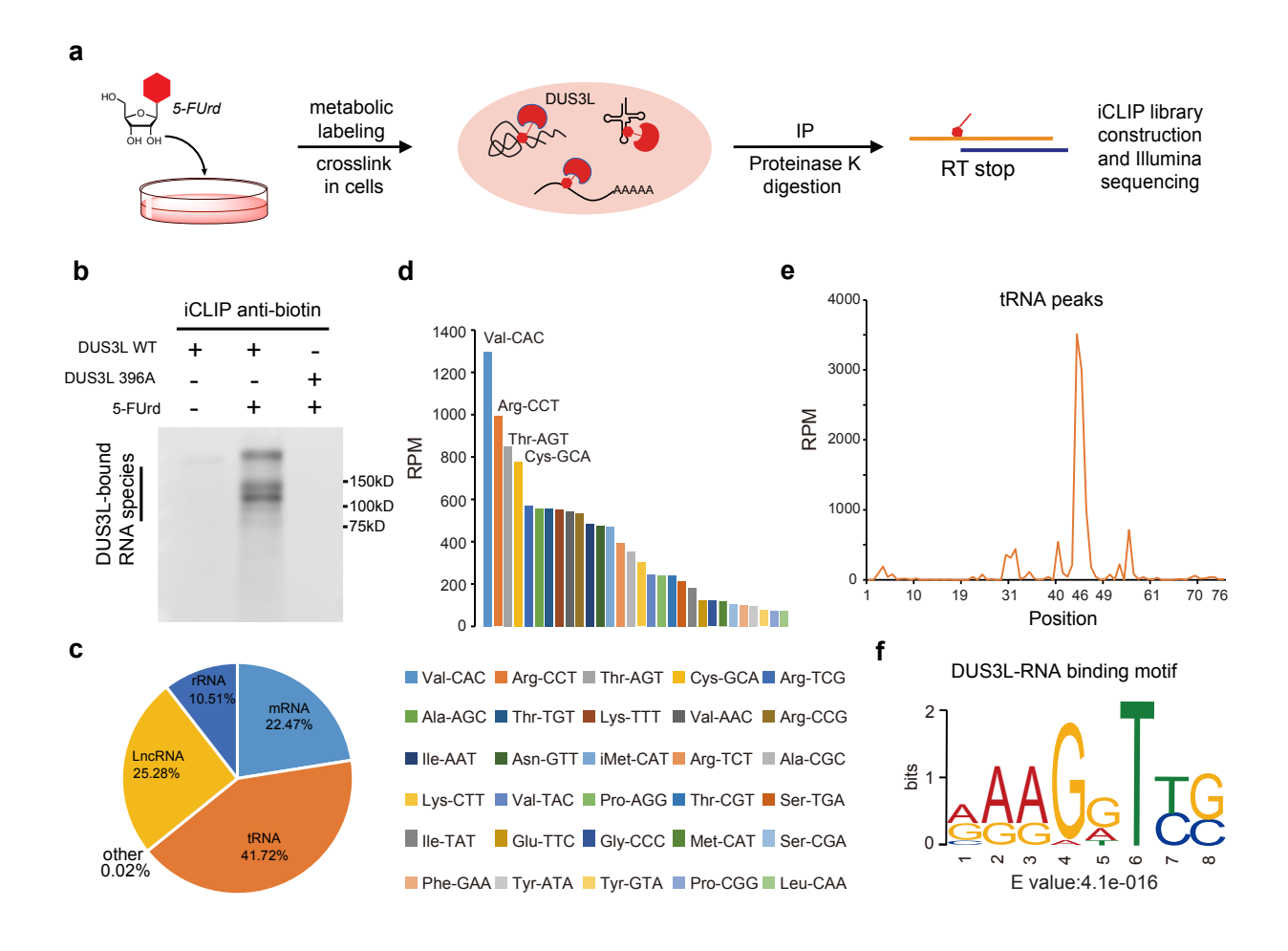


Figure 5. 5-FUrd-iCLIP sequencing of DUS3L substrates. **(a)** Schematic of 5-FUrd-iCLIP workflow. **(b)** Analysis of RNA-protein crosslinking in DUS3L iCLIP samples. Cells expressing DUS3L or DUS3L C396A were treated with 5-FUrd or left untreated, and covalently linked RNA was detected by anti-biotin western blot after immunoprecipitation and RNase fragmentation. For (b), the experiment was repeated 3 times independently with similar results. **(c)** Composition of RNA identified by 5-FUrd-iCLIP according to uniquely mapped reads. **(d)** Abundance of tRNA species as enriched by 5-FUrd-iCLIP; RPM: reads per million. **(e)** Coverage of all tRNA peaks according to their relative position within the mature tRNA. **(f)** Consensus motif detected by MEME using all RNA peaks identified by 5-FUrd-iCLIP.

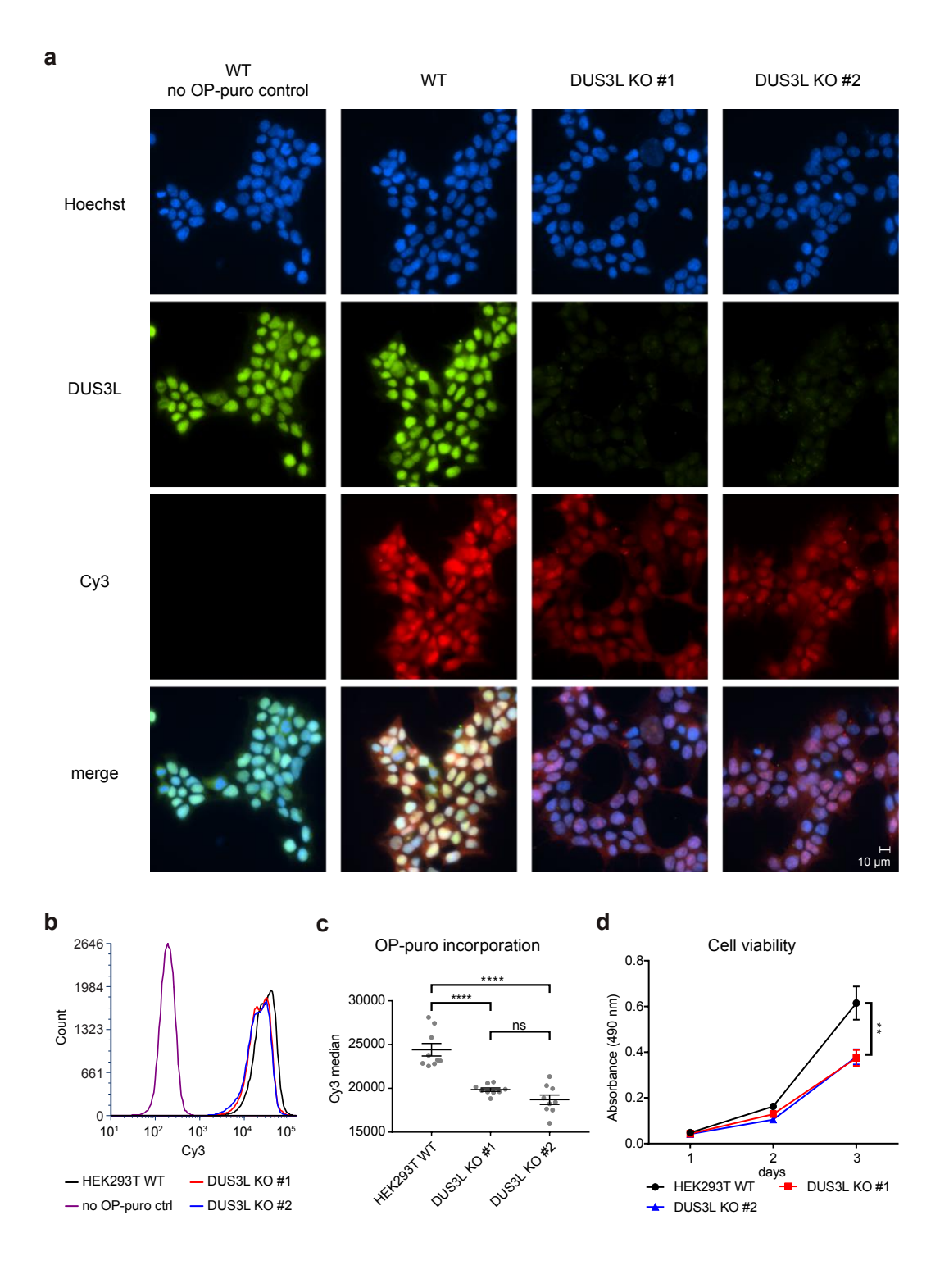


Figure 6. DUS3L regulates cell proliferation and protein translation efficiency. (a) Fluorescence microscopy analysis of DUS3L localization and OP-puro incorporation by WT and DUS3L KO cells. OP-puro labeling was imaged following CuAAC reaction with Cy3-azide. 2 independent biological replicates were analyzed for each cell line with similar results. (b) Flow cytometry analysis of global protein translation using OP-puro in WT and DUS3L KO cells (c) Plot of OP-puro incorporation as measured by Cy3 fluorescence from (b). The median fluorescence intensity and SEM from 3 independent biological replicates (50,000 cells analyzed per sample, 3 technical replicates per sample) are shown. Unpaired t test (two-tailed) was performed to evaluate the statistical significance. ****: p = 0.00013 (#1) and p = 0.0000094 (#2); ns: p = 0.064. (d) Cell viability of WT and DUS3L KO cells measured by MTS assay. 12 independent biological replicates were analyzed. Data represent mean values \pm SEM. Unpaired t test (two-tailed) was performed to evaluate the statistical significance. **: p = 0.0075 (#1) and p = 0.0068 (#2).

References

- 1. Boccaletto, P. et al. MODOMICS: a database of RNA modification pathways. 2017 update. *Nucleic Acids Res* **46**, D303-D307 (2018).
- 2. Nachtergaele, S. & He, C. The emerging biology of RNA post-transcriptional modifications. *RNA Biol* **14**, 156-163 (2017).
- 3. Roundtree, I.A., Evans, M.E., Pan, T. & He, C. Dynamic RNA Modifications in Gene Expression Regulation. *Cell* **169**, 1187-1200 (2017).
- 4. Delaunay, S. & Frye, M. RNA modifications regulating cell fate in cancer. *Nat Cell Biol* **21**, 552-559 (2019).
- 5. Li, X., Xiong, X. & Yi, C. Epitranscriptome sequencing technologies: decoding RNA modifications. *Nat Methods* **14**, 23-31 (2016).
- 6. Zaccara, S., Ries, R.J. & Jaffrey, S.R. Reading, writing and erasing mRNA methylation. *Nat Rev Mol Cell Biol* **20**, 608-624 (2019).

- 7. Cravatt, B.F., Wright, A.T. & Kozarich, J.W. Activity-based protein profiling: from enzyme chemistry to proteomic chemistry. *Annu Rev Biochem* **77**, 383-414 (2008).
- 8. Castello, A. et al. Insights into RNA biology from an atlas of mammalian mRNA-binding proteins. *Cell* **149**, 1393-1406 (2012).
- 9. Baltz, A.G. et al. The mRNA-bound proteome and its global occupancy profile on protein-coding transcripts. *Molecular cell* **46**, 674-690 (2012).
- 10. Pappireddi, N., Martin, L. & Wuhr, M. A Review on Quantitative Multiplexed Proteomics. *Chembiochem* **20**, 1210-1224 (2019).
- 11. Konig, J. et al. iCLIP reveals the function of hnRNP particles in splicing at individual nucleotide resolution. *Nat Struct Mol Biol* **17**, 909-915 (2010).
- 12. Liu, Y. & Santi, D.V. m5C RNA and m5C DNA methyl transferases use different cysteine residues as catalysts. *Proc Natl Acad Sci U S A* **97**, 8263-8265 (2000).
- 13. Khoddami, V. & Cairns, B.R. Identification of direct targets and modified bases of RNA cytosine methyltransferases. *Nat Biotechnol* **31**, 458-464 (2013).
- 14. Lu, L.J., Tseng, W.C. & Randerath, K. Effects of 5-fluorocytidine on mammalian transfer RNA and transfer RNA methyltransferases. *Biochem Pharmacol* **28**, 489-495 (1979).
- 15. Hussain, S. et al. NSun2-mediated cytosine-5 methylation of vault noncoding RNA determines its processing into regulatory small RNAs. *Cell Rep* **4**, 255-261 (2013).
- 16. Huang, T., Chen, W., Liu, J., Gu, N. & Zhang, R. Genome-wide identification of mRNA 5-methylcytosine in mammals. *Nat Struct Mol Biol* **26**, 380-388 (2019).
- 17. Yang, X. et al. 5-methylcytosine promotes mRNA export NSUN2 as the methyltransferase and ALYREF as an m(5)C reader. *Cell Res* **27**, 606-625 (2017).
- 18. Thompson, A. et al. Tandem mass tags: A novel quantification strategy for comparative analysis of complex protein mixtures by MS/MS. *Analytical Chemistry* **75**, 1895-1904 (2003).
- 19. Schosserer, M. et al. Methylation of ribosomal RNA by NSUN5 is a conserved mechanism modulating organismal lifespan. *Nat Commun* **6**, 6158 (2015).
- 20. Heissenberger, C. et al. Loss of the ribosomal RNA methyltransferase NSUN5 impairs global protein synthesis and normal growth. *Nucleic Acids Res* **47**, 11807-11825 (2019).
- 21. Herdy, B. et al. Analysis of NRAS RNA G-quadruplex binding proteins reveals DDX3X as a novel interactor of cellular G-quadruplex containing transcripts. *Nucleic Acids Res* **46**, 11592-11604 (2018).
- 22. Tuorto, F. et al. RNA cytosine methylation by Dnmt2 and NSun2 promotes tRNA stability and protein synthesis. *Nat Struct Mol Biol* **19**, 900-905 (2012).
- 23. Xue, S. et al. Depletion of TRDMT1 affects 5-methylcytosine modification of mRNA and inhibits HEK293 cell proliferation and migration. *Biochem Biophys Res Commun* **520**, 60-66 (2019).
- 24. Nordlund, M.E., Johansson, J.O., von Pawel-Rammingen, U. & Bystrom, A.S. Identification of the TRM2 gene encoding the tRNA(m5U54)methyltransferase of Saccharomyces cerevisiae. *RNA* **6**, 844-860 (2000).

- 25. Carter, J.M. et al. FICC-Seq: a method for enzyme-specified profiling of methyl-5-uridine in cellular RNA. *Nucleic Acids Res* **47**, e113 (2019).
- 26. Powell, C.A. & Minczuk, M. TRMT2B is responsible for both tRNA and rRNA m5U-methylation in human mitochondria. *RNA Biol* **17**, 451-462 (2020).
- 27. Cheng, Q.Y. et al. Chemical tagging for sensitive determination of uridine modifications in RNA. *Chem Sci* **11**, 1878-1891 (2020).
- 28. Lu, Z.H., Zhang, R. & Diasio, R.B. Purification and characterization of dihydropyrimidine dehydrogenase from human liver. *J Biol Chem* **267**, 17102-17109 (1992).
- 29. Xing, F., Hiley, S.L., Hughes, T.R. & Phizicky, E.M. The specificities of four yeast dihydrouridine synthases for cytoplasmic tRNAs. *J Biol Chem* **279**, 17850-17860 (2004).
- 30. Schweizer, U., Bohleber, S. & Fradejas-Villar, N. The modified base isopentenyladenosine and its derivatives in tRNA. *RNA Biol* **14**, 1197-1208 (2017).
- 31. Wiener, D. & Schwartz, S. The epitranscriptome beyond m(6)A. *Nat Rev Genet* **22**, 119-131 (2021).
- 32. Yu, F. et al. Molecular basis of dihydrouridine formation on tRNA. *Proc Natl Acad Sci U S A* **108**, 19593-19598 (2011).
- 33. Rider, L.W., Ottosen, M.B., Gattis, S.G. & Palfey, B.A. Mechanism of dihydrouridine synthase 2 from yeast and the importance of modifications for efficient tRNA reduction. *J Biol Chem* **284**, 10324-10333 (2009).
- 34. Huppertz, I. et al. iCLIP: protein-RNA interactions at nucleotide resolution. *Methods* **65**, 274-287 (2014).
- 35. Frith, M.C. et al. A code for transcription initiation in mammalian genomes. *Genome Res* **18**, 1-12 (2008).
- 36. Bailey, T.L. et al. MEME SUITE: tools for motif discovery and searching. *Nucleic Acids Res* **37**, W202-208 (2009).
- 37. Liu, J., Xu, Y., Stoleru, D. & Salic, A. Imaging protein synthesis in cells and tissues with an alkyne analog of puromycin. *Proc Natl Acad Sci U S A* **109**, 413-418 (2012).
- 38. Kato, T. et al. A novel human tRNA-dihydrouridine synthase involved in pulmonary carcinogenesis. *Cancer Res* **65**, 5638-5646 (2005).
- 39. Schaefer, M. et al. RNA methylation by Dnmt2 protects transfer RNAs against stress-induced cleavage. *Genes Dev* **24**, 1590-1595 (2010).
- 40. Bohnsack, K.E., Hobartner, C. & Bohnsack, M.T. Eukaryotic 5-methylcytosine (m(5)C) RNA Methyltransferases: Mechanisms, Cellular Functions, and Links to Disease. *Genes (Basel)* **10** (2019).
- 41. Kuchino, Y. & Borek, E. Tumour-specific phenylalanine tRNA contains two supernumerary methylated bases. *Nature* **271**, 126-129 (1978).
- 42. Madison, J.T. & Holley, R.W. The Presence of 5,6-Dihydrouridylic Acid in Yeast "Soluble" Ribonucleic Acid. *Biochem Biophys Res Commun* **18**, 153-157 (1965).
- 43. Xing, F., Martzen, M.R. & Phizicky, E.M. A conserved family of Saccharomyces cerevisiae synthases effects dihydrouridine modification of tRNA. *RNA* **8**, 370-381 (2002).

- 44. Bishop, A.C., Xu, J., Johnson, R.C., Schimmel, P. & de Crecy-Lagard, V. Identification of the tRNA-dihydrouridine synthase family. *J Biol Chem* **277**, 25090-25095 (2002).
- 45. Alexandrov, A. et al. Rapid tRNA decay can result from lack of nonessential modifications. *Molecular cell* **21**, 87-96 (2006).
- 46. Lanning, B.R. et al. A road map to evaluate the proteome-wide selectivity of covalent kinase inhibitors. *Nat Chem Biol* **10**, 760-767 (2014).
- 47. Backus, K.M. et al. Proteome-wide covalent ligand discovery in native biological systems. *Nature* **534**, 570-574 (2016).
- 48. Erlanson, D.A. et al. Site-directed ligand discovery. *Proc Natl Acad Sci U S A* **97**, 9367-9372 (2000).
- 49. Trendel, J. et al. The Human RNA-Binding Proteome and Its Dynamics during Translational Arrest. *Cell* **176**, 391-403 e319 (2019).

Data availability statement

The sequencing data reported in this paper has been deposited in the NCBI Gene expression omnibus (accession code: GSE175825). The proteomics data reported in this paper is available via ProteomeXchange with identifier PXD022645. Source data are provided with this paper.

Online Methods

Chemicals

5-Azacytyidine (5-AzaC), 5-fluorocytidine (5-FCyd), 5-fluorouridine (5-FUrd), 5-chlorocytidine (5-ClCyd), 5-chlorouridine (5-ClUrd), 5-bromocytidine (5-BrCyd), and 5-bromouridine (5-BrUrd) were all purchased from Carbosynth. All other chemicals were purchased from Sigma-Aldrich or Fisher Scientific unless otherwise indicated.

Plasmids

NSUN2, NSUN5, NSUN6, TRMT2A, DNMT2, and DUS3L cDNA were obtained from Dharmacon (#MHS6278-213243840, #MHS6278-202826182, #MHS6278-202802090, #MHS6278-202760193, #MHS6278-202756140, and #MHS6278-202830580). The C396A mutation was introduced into DUS3L using overlap extension PCR with mutagenic primers. For transient transfection and construction of Flp-In cell lines, NSUN2, NSUN5, NSUN6, TRMT2A, DNMT2, and DUS3L cDNA were cloned into a modified pcDNA5/FRT/TO (Life Technologies #V6520-20) vector containing an N-terminal 3x-FLAG tag. For generation of the KO cell lines, DNA oligos containing guide RNA sequences were cloned into pX330-U6-Chimeric_BB-CBh-hSpCas9 (Addgene #42230).

The DNA oligos were phosphorylated with T4 PNK (NEB # M0201), annealed, and ligated into *BbsI* (NEB #R3539) digested px330 backbone with T4 DNA ligase (NEB # M0202).

General cell culture

HEK293T WT and KO cells were cultured at 37 °C in a humidified atmosphere with 5% CO₂ in DMEM (Thermo Fisher #11995073) supplemented with 10% fetal bovine serum (Bio-Techne #S12450H), 1x penicillin-streptomycin (Thermo Fisher #15070-063) and 2 mM L-glutamine (Thermo Fisher #25030-081).

Generation of stable cell lines

To generate stable cell lines expressing 3xFLAG-tagged NSUN2, NSUN5, and TRMT2A, the Flp-In T-Rex 293 cells were seeded at 0.6 million cells per well in 6-well plates, and co-transfected with pOG44 (2 μ g, Thermo Fisher #V600520) and pcDNA5/FRT/TO plasmid containing 3xFLAG-NSUN2, NSUN5, or TRMT2A (0.2 μ g). Following selection in 100 μ g/mL hygromycin B and 15 μ g/mL blasticidin, colonies were expanded. To test the expression efficiency of 3xFLAG-tagged constructs, cells were induced with tetracycline (0 to 1 μ g/mL) for 24 h. Cells were harvested and lysed in cell extraction buffer (Invitrogen #FNN0011, added freshly: 1 mM PMSF and protease inhibitor tablet Sigma #11836170001). The proteins were separated on SDS-PAGE gel and analyzed by western blot (anti-FLAG M2, 1: 1000 dilution, Sigma # F1804).

Generation of knockout cell lines

0.8 million HEK293T WT cells were seeded in 6-well cell culture dish the day before transfection. 2 μg of px330 plasmid containing the gRNA for the target protein and 200 ng of pcDNA3-FKBP-EGFP-HOTag3 (Addgene #106924) were co-transfected using Lipofectamine 2000 (Thermo Scientific #11668027). Cells were sorted by FACS two days post-transfection. Top 95% cells displaying GFP signals were sorted as single cells into 96-well dishes. Genomic PCR and western blot (anti-NSUN2 Proteintech #20854-1-AP, 1:2000; anti-NSUN5 Proteintech #15449-1-AP, 1:2000; anti-TRMT2A Proteintech #16199-1-AP, 1:1000; anti-DUS3L Proteintech #15643-1-AP, 1:2000; anti-β actin Cell Signaling #8H10D10, 1:10000 as loading control) were performed to confirm knockout.

PolyA pulldown of 5-FCyd treated cells for mass spectrometry

HEK293T cells were treated with 10 μ M 5-FCyd at 80% confluency for 12 h. Cells from 10 x 10 cm dishes were used per replicate. PolyA pulldown was performed following literature precedent^{8, 9} with minor modifications. 10 mL of lysis buffer (20 mM Tris, pH7.5, 500 mM LiCl, 0.5% LiDS, 1 mM EDTA, added freshly: protease inhibitor tablet (Sigma #11836170001) and 5 mM DTT) and 750 μ L of pre-equilibrated oligo d(T)₂₅ magnetic beads (NEB # S1419S) were used per sample. Lysis, pulldown, and washes were performed at room temperature. Buffers used for washing were lysis buffer, NP-40 wash buffer (20 mM Tris, pH 7.5, 140 mM LiCl, 1 mM EDTA, 0.5% NP-40 (v/v), added freshly: 0.5 mM DTT), and NP-40-free wash buffer (20 mM HEPES, pH 7.5, 140 mM LiCl, 1 mM EDTA, added freshly: 0.5 mM DTT). The bound polyA RNA was eluted in 350 μ L of elution buffer (20 mM HEPES, pH 7.5, 1 mM EDTA) by heating at 55 °C for 3 min. 250 units of Benzonase Nuclease (Millipore Sigma #70746) was added to concentrated eluate and

incubated at 37 °C for 1 h to release the crosslinked proteins from RNA. The protein concentration in the samples was determined by BCA assay (Thermo Scientific #23225).

Mass spectrometry-based proteomics

Samples were mostly prepared as previously described 50 . Eluted samples were dried using a vacuum evaporator at room temperature (RT) and taken up with 10 μ L 6 M guanidinium chloride in 200 mM EPPS pH 8.0 to the final concentration of 0.2 μ g/ μ L. The samples were subsequently digested with 20 ng/uL Lys-C (Wako), 10 ng/ μ L trypsin (Promega), and labeled with TMT6-plex (Thermo Fisher Scientific), and cleaned up for LC-MS analysis with stage tips 51 . Approximately 2 μ g of the sample was analyzed via LC-MS on an Orbitrap Fusion Lumos with a TMT-MS2 method as previously described

Mass Spectrometry-based proteomics data analysis

Mass Spectrometry data analysis was performed essentially as previously described ⁵³, ⁵⁴. The mass spectrometry data in the Thermo RAW format was analyzed using the Gygi Lab software platform (GFY Core Version 3.8) licensed through Harvard University. The ratio in each channel was normalized by the channel's median change for the following proteins, which are experimentally expected to be the same across the conditions: SRSF3, SNRPE, SRSF10, SRSF1, SRSF4, CPSF1, SRSF7, SNRPB, SNRPF, SNRPD2, ZRANB2, POLRMT, TROVE2, FAM120A, SLTM, GEMIN5, MTPAP, MRPL43, SNRPD1. The normalized values are then subjected to downstream statistical analysis.

RNABPP validation by western blot

For NSUN2, NSUN5, and TRMT2A, Flp-In T-Rex 293 cell lines expressing the 3xFLAG-tagged proteins were used to validate the proteomics results. For DUS3L, HEK293T WT cells were used. 5-FCyd treatment was performed as described previously. For polyA pulldown, washes with NP-40-free buffer were omitted and RNase cocktail (Invitrogen #AM2288) instead of Benzonase was used for RNA digestion. The eluates were separated on an SDS-PAGE gel and analyzed by western blot.

Gel-based crosslinking assay

For gel based cross-linking assay, 3xFLAG-tagged proteins were expressed by transient transfection in HEK293T cells or by tetracycline induction in the corresponding Flp-In T-Rex 293 cell lines for NSUN2, NSUN5, NSUN6, DNMT2, and TRMT2A. For DUS3L, HEK293T WT cells were used for the cross-linking of DUS3L with the panel of 5-halogenated pyrimidine compounds. To test the cross-linking between DUS3L C396A mutant and the uridine analogs, WT and DUS3L C396A were expressed in DUS3L KO cells by transient transfection. 12 h treatment was performed for all cell lines and compounds at the indicated concentrations. Cells were lysed in cell extraction buffer (Invitrogen), and the proteins were separated on a 10% SDS-PAGE gel followed by western blot analysis.

RNA isolation and nucleoside LC-MS/MS

Total RNA was extracted using TRIzol reagent (Thermo Fisher #15596018) following the manufacturer's protocol. Small RNA was isolated using Zymo RNA Clean & Concentrator-5 (Zymo Research # R1016) following the manufacturer's protocol with minor modification (adjusted RNA binding buffer was made by mixing 3 parts of RNA binding buffer and 2 parts of EtOH). For mRNA isolation, total RNA was subjected to two rounds of polyA selection using Oligo-d(T)25 beads (NEB #S1419S). The polyA RNA was further subjected to ribo-depletion to remove ribosomal RNA contamination using the NEBNext rRNA Depletion Kit (NEB #E6310) or custom synthesized probes⁵⁵. Small RNA was removed from ribo-depleted polyA RNA using Zymo RNA Clean & Concentrator-5 (Zymo Research). The RNA was digested and dephosphorylated with nuclease P1 (Wako USA #145-08221) and Antarctic phosphatase (NEB #M0289) prior to LC-MS analysis. Briefly, 5 – 10 μg of RNA was digested in a 30 μL reaction with 2 units of nuclease P1 at 37 °C for 2 h (buffer composition: 7 mM NaOAc pH 5.2, 0.4 mM ZnCl₂). Dephosphorylation was performed next by adding 1.5 µL of Antarctic phosphatase and 3.5 µL of 10x Antarctic phosphatase buffer and incubating the reaction at 37 °C for another 2 h. Dynamic multiple reaction monitoring (DMRM) method was employed to perform quantitative LC-QQQ-MS analysis of modified nucleosides on an Agilent 1260 Infinity II HPLC coupled to an Agilent 6470 triple quadrupole mass spectrometer in positive ion mode. A Hypersil GOLD C18 Selectivity HPLC Column (Thermo Fisher #25003-152130; 3 µm particle size, 175 Å pore size, 2.1 x 150 mm; 36 °C) was used for all analyses, with a gradient composed of 0.1 % formic acid in H₂O (A) and acetonitrile (B) at a flow rate of 0.4 mL/min following literature precedent⁵⁶. The operating parameters for the mass spectrometer were as follows: gas temperature 325 °C; gas flow 12 L/min; nebulizer 20 psi and capillary voltage 2500 V,

with fragmentor voltage and collision energy optimized for each nucleoside. MS1 (parent ion) to MS2 (deglycosylated base ion) transition for each nucleoside was set as follows: m/z 262 \rightarrow 130 for 5-FCyd, m/z 262 \rightarrow 131 for 5-FUrd, m/z 258 \rightarrow 126 for m⁵C, m/z 259 \rightarrow 127 for m⁵U, m/z 247 \rightarrow 115 for DHU, m/z 336 \rightarrow 204 for i⁶A, m/z 268 \rightarrow 136 for A, m/z 244 \rightarrow 112 for C, and m/z 245 \rightarrow 113 for U. Commercially available ribonucleosides were used to generate standard curves. The levels of 5-FCyd, 5-FUrd, m⁵C, m⁵U, DHU, and i⁶A were determined by normalizing the concentration of modified nucleosides to the concentration of the corresponding canonical nucleosides in the sample.

5-FUrd-iCLIP

Library preparation for iCLIP was adapted from the literature³⁴. Flp-In T-Rex 293 cells expressing 3xFLAG-DUS3L (20 x 10 cm with 5-FUrd treatment and 40 x 10 cm for untreated control) were treated with 1 μg/mL tetracycline once the cells reached 60% confluency. After 12 hr, the medium was changed to fresh medium containing 1 μg/mL tetracycline (control) or 1 μg/mL tetracycline and 100 μM 5-FUrd and cultured for another 12 hr. Cells were washed twice with cold PBS and then 500 μL lysis buffer (50 mM Tris–HCL pH 7.4, 100 mM NaCl, 1% NP-40, 0.1% SDS and 0.5% sodium deoxycholate) was added to each dish. Lysates were treated with Turbo DNase (AM2239) and a low (1:200) or high (1:50) concentration of RNasel (AM2295) at 37 °C for 3 mins with rotation after which they were centrifuged at 13000 rpm for 15 min at 4°C. The supernatant was incubated with anti-FLAG beads (200 μL Protein G beads and 15 μg anti-FLAG M2 antibody) at 4 °C overnight with rotation, and the immunoprecipitated material was then washed 3 times with high-salt buffer and then once with CutSmart buffer (NEB). The

beads were treated with Quick-CIP (NEB) at 37 °C for 30 mins with rotation, washed twice with high-salt buffer, and then incubated with preadenylated and biotin labeled L3 linker by using T4 RNA ligase I (NEB) at 16 °C overnight. After washing 3 times with high-salt buffer, the beads were boiled with 60 µL sample buffer and 3 µL was analyzed by western blot for biotinylation with the chemiluminescent nucleic acid detection module (Thermo). The rest of the sample was gel purified based on the position of the biotin signal. Immunoprecipitated RNA was recovered using D-tube dialyzer midi (Merck-Millipore) and digested with proteinase K (Roche). Reverse transcription was performed using oligonucleotides containing randomized barcodes (UMIs) and two inversely oriented adaptor regions separated by a BamHI restriction site. cDNAs were size-purified (70-80 nt, 80-100 nt and 100-150 nt) on TBE-Urea gels and then circularized by CircLigase II (Epicentre). Circularized cDNAs were digested with BamHI and linearized cDNAs were amplified using Solexa primers and submitted for Illumina sequencing.

Bioinformatic analysis

The iCLIP data was processed using the iCount Primary Analysis pipeline (consensus mapping) on iMAPs web server (https://imaps.genialis.com/iclip). Briefly, random unique molecular identifiers were used to distinguish and discard PCR duplicate reads, and adaptor/barcode sequences were then removed. Trimmed reads were first mapped to tRNA/rRNA with STAR (v.2.7.0f). The unmapped reads were further mapped to GRCh38 with STAR (v.2.7.0f) and only uniquely mapping reads were used for further analysis. iCount generated raw cross-linking sites were used for peak calling analysis by Paraclu with the following parameters: minimal sum of scores inside a cluster = 10; maximal

cluster size = 4; minimal density increase = 2. Read counts were normalized per million uniquely mapping reads (RPM). Peaks that were unique to the 5-FUrd-treated sample or showed fold change > 4 (5-FUrd treatment vs control) were kept as significant peaks after intersection. Only significant peaks with read counts >10 in at least two out of three replicates were selected for further analyses. Sequences 5 bases up and down-stream were extracted from the reference and used for motif analysis by MEME (V.5.3.3) using -mod zoops -nmotifs 3 -minw 6 -maxw 50 -objfun classic -revcomp -markov order 0.

Global protein translation assay

The global protein translation efficiency in HEK293T WT and DUS3L KO cells were assessed using O-propargyl-puromycin (OP-puro; Click chemistry tool #1407-5) based on literature precedent⁵⁷. In brief, the cells were labeled with OP-puro by replacing the medium with fresh medium containing 50 μM OP-puro (20 mM reconstituted stock solution in DMSO) and incubating the cells at 37 °C for 1 h. Cells incubated in fresh medium without OP-puro were used as negative control. Cu(I)-catalyzed azide/alkyne cycloaddition was performed to conjugate OP-puro to Cy3-azide (Click chemistry tools #AZ119-1) on fixed cells: cells were resuspend in PBS containing 1 mM Cu(II)SO₄, 2 mM THPTA, 10 μM Cy3-azide, and 10 mM sodium ascorbate (freshly prepared), and incubated at room temperature for 2 h in the dark. The reaction solution was removed at the end of the reaction and cells were washed with ice-cold PBST for 3 times. The cells were then resuspended in PBS containing Hoechst 33342 (Thermo Scientific # 62249, 20 μg/mL) and kept on ice and protected from light until flow cytometry analysis (less than 24 h). Each single cell suspension was run on the BD LSRII SORP Flow Cytometer (BD

Biosciences, San Jose, CA). The fluorescent Cy3 was excited by a 561nm, 40 mW laser and its emitted light was detected after passing through a 582/15 bandpass filter. The fluorescent Hoechst 33342 was excited by a 355 nm, 30 mW laser and its emitted light was detected after passing through a 450/50 bandpass filter. To confirm consistency among cytometer runs, each sample and control was run on the cytometer three times, producing three replicate raw data files for each. On an FSC-A (Forward Scatter-Area) vs. SSC-A (Side Scatter-Area) scatter plot, only cells were included in the primary analysis gate. On an FSC-A (Forward Scatter- Area) vs. FSC-H (Forward Scatter-Height) scatter plot, only single cells were included in the secondary analysis gate. The tertiary analysis gate further excluded aggregates on a scatter plot of the Hoechst 33342 width value vs. the Hoechst 33342 area fluorescence intensity. Each raw data file contained the aforementioned fluorescence and scatter values of 50,000 single cells. The Hoechst 33342 area fluorescence intensities of all cells in the tertiary gate were plotted on a histogram to represent DNA content of each cell. The Cy3 area fluorescence intensities of the same cell population were plotted on another histogram to represent the quantity of Cy3 present in each cell. The raw data files were analyzed in BD FACSDiva software version 8.0.2 (BD Biosciences, San Jose, CA.) and FCS Express Version 7 (DeNovo Software, Pasadena, CA.). The median fluorescence intensities of Cy3 from each cytometer runs were used to compare the global protein translation efficiency among the corresponding cell lines.

Fluorescence microscopy

For fluorescence microscopy experiment, a poly-L-lysine (Sigma #P8920) coated 12 mm glass coverslip was placed in each well before cell seeding. The OP-puro labeling was performed as described previously. At the end of the labeling, cells were washed once with DPBS, and fixed with 3 % PFA in PBS for 20 min at room temperature and washed with PBS for 3 times. The cells were then permeabilized with PBST for 20 min at room temperature and washed twice with PBS. Click chemistry with Cy3-azide was performed as described in the previous section. Coverslips were incubated upside down with drops (100 µL) of freshly prepared reaction mixture. The reaction was allowed to proceed for 2 hr at room temperature in the dark. Cells were then washed 5 time with PBST for 10 min to remove non-specific binding. To stain for DUS3L, cells were blocked with 5% goat serum in PBST for 1 hr. The coverslips were incubated with anti-DUS3L antibody (Proteintech #15643-1-AP, 1:200) for 2 hr and washed with PBST (0.1% Triton X-100 in PBS) 3 times for 5 min each. Goat-anti-rabbit Alexa 488 antibody (Jackson ImmunoResearch, 1:400) for 1 hr was used for secondary antibody staining. The cells were washed twice with PBST for 5 min, stained with Hoechst 33342 (Thermo Scientific, 1 μg/mL) for 5 min, and washed with PBS twice for 5 min. The coverslips were mounted in ProLong Gold AntiFade Reagent (Life Technologies) and sealed with nail polish. Images of fixed cells were acquired using NIS Elements AR software and a Nikon Eclipse Ti microscope equipped with 100x objective and CMOS camera. Images used for direct comparison were acquired using standardized illumination and exposure settings and displayed with identical lookup table (LUT) settings.

Cell viability assay

HEK293T WT and DUS3L KO cells were plated in 96-well culture plates (4000 cells in 200 μL of medium per well) on day 0. Cell viability was measured daily using the MTS assay (CellTiter 96 Aqueous Non-Radioactive Cell Proliferation Assay; Promega # G5430) for a total of three days (day 1 – day 3). The absorbance was read at 490 nm using a Synergy H1 Microplate Reader (BioTek).

Methods-only References

- 50. Gupta, M., Sonnett, M., Ryazanova, L., Presler, M. & Wuhr, M. Quantitative Proteomics of Xenopus Embryos I, Sample Preparation. *Methods Mol Biol* **1865**, 175-194 (2018).
- 51. Rappsilber, J., Mann, M. & Ishihama, Y. Protocol for micro-purification, enrichment, pre-fractionation and storage of peptides for proteomics using StageTips. *Nat Protoc* **2**, 1896-1906 (2007).
- 52. Sonnett, M., Yeung, E. & Wuhr, M. Accurate, Sensitive, and Precise Multiplexed Proteomics Using the Complement Reporter Ion Cluster. *Anal Chem* **90**, 5032-5039 (2018).
- 53. Sonnett, M., Gupta, M., Nguyen, T. & Wuhr, M. Quantitative Proteomics for Xenopus Embryos II, Data Analysis. *Methods Mol Biol* **1865**, 195-215 (2018).
- 54. Huttlin, E.L. et al. A tissue-specific atlas of mouse protein phosphorylation and expression. *Cell* **143**, 1174-1189 (2010).
- 55. Adiconis, X. et al. Comparative analysis of RNA sequencing methods for degraded or low-input samples. *Nat Methods* **10**, 623-629 (2013).
- 56. Su, D. et al. Quantitative analysis of ribonucleoside modifications in tRNA by HPLC-coupled mass spectrometry. *Nat Protoc* **9**, 828-841 (2014).
- 57. Hidalgo San Jose, L. & Signer, R.A.J. Cell-type-specific quantification of protein synthesis in vivo. *Nat Protoc* **14**, 441-460 (2019).